Marine Pollution Bulletin 228 (2026) 119590

Contents lists available at ScienceDirect

Marine Pollution Bulletin

journal homepage: www.elsevier.com/locate/marpolbul

Large prevalence of cellulosic fibers in the first-year sea ice from Amur Bay, Sea of Japan

Davide Riseri [a], Irina Chubarenko [b], Alexander Lazaryuk [c], Marina Lasagni [a], Elena Collina [a], Francesco Saliu [a,*]

[a] Earth and Environmental Science Department, University of Milano-Bicocca, Piazza Della Scienza 1, 20123, Milano, Italy
[b] Shirshov Institute of Oceanology, Russian Academy of Sciences, 36 Nakhimovsky Prosp., Moscow, 117997, Russia
[c] Il'ichev Pacific Oceanological Institute, Russian Academy of Sciences, 43 Baltiyskaya str., Vladivostok, 690041, Russia

ARTICLE INFO

Keywords:
Sea ice
Microfibers
Pollution
Microplastic
Sea of Japan

ABSTRACT

The contamination of sea ice by microplastics (MPs) and microfibers (MFs) is still underexplored. In this study, we report the abundance, chemical composition, and vertical distribution of MPs and MFs in the seasonal sea ice of Amur Bay (Sea of Japan, Russia). More specifically, three ice cores (38–53 cm long) were manually extracted, sectioned into ~5 cm layers, melted, and filtered without chemical pretreatment and then submitted to μFTIR analysis. A total of 29 filters, corresponding to ~24.5 kg of sea ice, were analyzed. Overall, 6026 anthropogenic items in the 25–5000 μm size range were identified, yielding a bulk mean of 4716 ± 2509 items/L. Among them, 94.7% were fibers, 4.1% fragments, and 1.2% films. Particles between 0.3 and 5 mm represented over 80% of the total, while smaller particles were less abundant. Notably, 90% of fibers were cellulose-based. MPs averaged 685 ± 550 items/L and consisted mainly of polyester (47%), acrylic (25%), polyethylene (4%), and polystyrene (3%). Core T15-K4 exhibited significant stratification, with fibers concentrated in the middle layers, whereas T13-K1 and T15-K2 showed no significant vertical variation. These findings indicate that first-year sea ice functions as a temporary sink for anthropogenic particulate pollutants. The strong predominance of cellulosic MFs underscores the need to include natural and semi-synthetic fibers in future monitoring efforts.

1. Introduction

Plastic pollution is a major global issue: plastics have been found in every marine and terrestrial environment and are considered a threat for vital marine ecosystems. One of the key challenges posed by plastic pollution lies in the fragmentation of plastics due to chemical and physical processes, which reduces particle size to MPs (<5 mm), enhances their environmental dispersal, and complicates the understanding of the fate of plastic litter in nature (Wayman and Niemann, 2021; Lyulin et al., 2025; Zhang et al., 2021). The presence of plastics and MPs poses a threat to marine organisms through direct physical interaction (Browne et al., 2008), as well as by transporting and leaching toxic substances (Cole et al., 2013; Isa et al., 2025). Both small and large particles can be ingested and enter the food web (Provencher et al., 2019), leading to the transfer of plastic pollutants across species. Recent studies have also highlighted the role of MPs in facilitating the long-term persistence of radionuclides in surface seawater. For instance, Ikenoue et al. (2022) demonstrated that MPs with adsorbed radiocesium may contribute to elevated $^{137}Cs/^{133}Cs$ ratios in zooplankton samples. In more general terms, understanding the distribution patterns of plastic and MPs is fundamental for risk assessment and risk mitigation plans. However, at the present time the research community is still facing the so-called "missing plastic" problem: global plastic production is around 414 Mt./year (PlasticsEurope, 2024), with approximately 9 Mt./year entering the oceans (Jambeck et al., 2015), yet "only" about 250,000 t are detected in surface waters (Eriksen et al., 2014; Thompson et al., 2004). This suggests that multiple sinks may exist within ocean systems. Direct observations have confirmed the operation of specific sinking pathways, such as the biological pump transporting microplastics to the deep ocean (Ikenoue et al., 2024), but our general understanding of other sinks remains limited.

While these challenges persist, a new concern has recently emerged: microfibers (MFs). From the very beginning of microplastic (MP) research, plastic MFs were classified as part of the microplastic family and consequently reported in plastic pollution studies. This classification was based on the assumption that most anthropogenic fibers in the

* Corresponding author.
E-mail address: francesco.saliu@unimib.it (F. Saliu).

https://doi.org/10.1016/j.marpolbul.2026.119590
Received 17 October 2025; Received in revised form 13 March 2026; Accepted 14 March 2026
Available online 19 March 2026

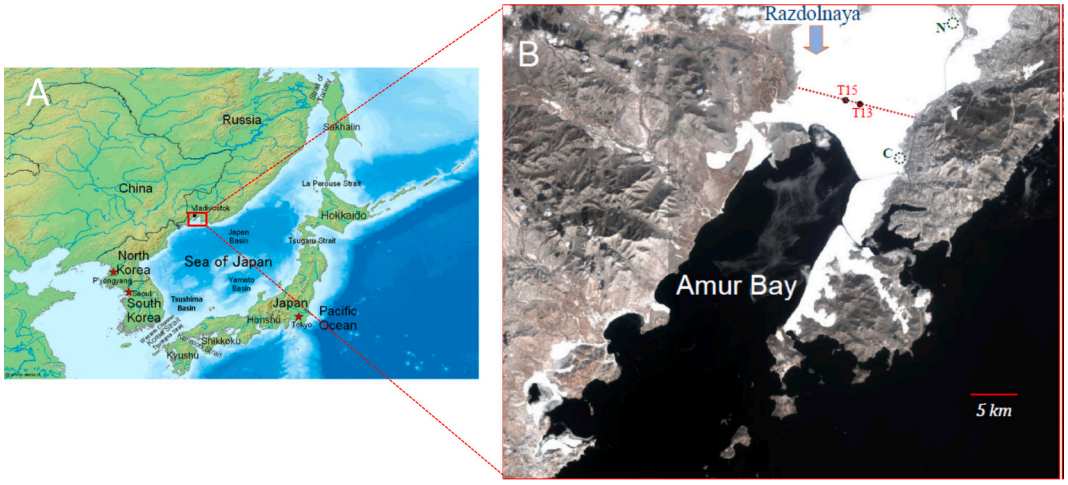

Fig. 1. Map of the sampling area: (A) Geographical location of Amur Bay; (B) Earth satellite image showing Amur Bay, captured on February 29, 2020. The locations of the cores for MPs are marked in red, while the locations of the cores used for salinity profiles are marked in light blue The dotted line between the shores of the bay also includes another 15 additional points for measuring under-ice water by the STD probe and ice parameters. The distance between the east and west points on the T-transect is about 13 km. Razdolnaya river and deepwater outfalls from wastewater treatment plants are shown: (N) in the north near the De-Friz Peninsula (discharge up to 15,000 m^3/day) and (C) in the central urban area (79,000 m^3/day). (For interpretation of the references to color in this figure legend, the reader is referred to the web version of this article.)

environment were synthetic. However, recent studies have revealed that the majority of MFs found in the world's oceans are not plastics but are composed of dyed cellulosic materials (Suaria et al., 2020). The predominance of cellulosic fibers has also been documented in other marine compartments, including seafloor sediments (e.g., Woodall et al., 2014; Sanchez-Vidal et al., 2018), marine biota (Remy et al., 2015; Taylor et al., 2016), as well as in terrestrial and freshwater systems (e.g., Dris et al., 2018) and in the atmosphere (e.g., Stanton et al., 2019). Recent studies further underscore the prevalence of these cellulosic materials in other environmental compartments and provided further analytical frameworks for their identification (Silva et al., 2024).

Overall, finding cellulosic fibers widespread recalls for a more careful revision of the assumption that only synthetic polymers pose an environmental threat. Although cellulose is inherently biodegradable, most cellulosic fibers in the environment originate from textile products containing chemical additives (e.g., dyes, formaldehyde resins, PFAS) that can both modify their persistency and also leach into water and sediments, acting as vectors for toxic substances (Remy et al., 2015; Sillanpää and Sainio, 2017; Athey et al., 2022; Ji et al., 2024). In addition, rowing evidence confirms that cellulosic fibers may induce biological harm comparable to, or in some cases exceeding, that of synthetics (Jolly et al., 2025). For instance, it was shown that the ingestion of cotton microfibers impairs juvenile invertebrate development (Siddiqui et al., 2023; dos Santos et al., 2024), while rayon increases oxidative stress and alters gut microbiomes in mussels (Jiang et al., 2024). Wool and cotton microfibers were shown to perturb digestive and immune functions in Pacific oysters, whereas synthetic fibers produced fewer measurable effects (Détrée et al., 2023). In terrestrial systems, viscose and lyocell are more toxic to earthworms than polyester (Courtene-Jones et al., 2024). Finally, the biodegradability of cellulosic fibers does not necessarily preclude environmental risk: degradation in marine and soil environments can be slow, and during this period they may persist as particulate pollutants that can be ingested by organisms and potentially exert harmful effects (Stanton et al., 2024).

As this recent literature indicates that non synthetic fibers are widely reported in many environmental studies and may also have potential ecotoxicological implications, some authors have suggested considering MFs as a distinct class of anthropogenic particulate contaminants rather than simply a subset of MPs (e.g., Liu et al., 2019).

However, at present there are no definitive analytical approaches to reliably distinguish naturally occurring fibers from anthropogenic ones, particularly among cellulose-based and protein-based fibers.. Researchers still largely rely on morphological and spectroscopic characterization, taking into account fiber diameter, color, and spectral features. Yet in many cases, the spectra of natural and man-made polymers are nearly identical. For example, distinguishing between natural and man-made cellulosic fibers (e.g. cotton vs Rayon, Viscose, Lyocell) using FTIR spectroscopy remains analytically challenging due to the high similarity of their spectra, particularly when dealing with environmentally weathered fibers (Suaria et al., 2020; Athey and Erdle, 2022). Analysis of standard reference has in fact already highlighted how the distinction relies on subtle differences in only a few absorption peaks observed in reference materials (Comnea-Stancu et al., 2017; Geminiani et al., 2022). Since these differences can easily be obscured by the presence of contaminants and/or partial oxidation in environmentally collected samples (Lusher et al., 2014; Peeken et al., 2018; Cai et al., 2019; Loof et al., 2016) is therefore a common practice to consider both natural and man-made cellulosics fibers in single category for the purpose of reporting the results. In addition, discoloration and fragmentation caused by environmental weathering further complicate the identification process, making the discrimination between natural and anthropogenic fibers particularly challenging.

Overall, the major challenge in this research field is still represented by the lack of standardized sampling protocols that has led to substantial variability in the abundance of particles reported across different studies (Suaria et al., 2020; Ivleva, 2021). Firstly, the high risk of airborne contamination during sampling and analysis makes the determination of MFs even more challenging than that of MPs, which is one of the main reasons why fibers have been excluded from many MP surveys (see, e.g., Woodall et al., 2015; Suaria et al., 2016). The choice of sampling equipment has also strongly influenced the results. For instance, manta nets are ineffective at retaining fibers during collection and may introduce background contamination. As an alternative, Suaria et al. (2020) proposed the use of pre-rinsed stainless-steel buckets to minimize contamination and improve fiber recovery. Finally, differences in chemical treatment protocols can also significantly affect outcomes. Many MP studies use hydrogen peroxide (H_2O_2, 30%) digestion to remove organic matter (e.g., Peeken et al., 2018; Kim et al., 2021; Ohno et al., 2024). However, this strong oxidizing agent may degrade not only organic debris but also weathered polymers such as polyester and cellulosic materials, which are particularly susceptible to oxidation

(Chubarenko et al., 2022). While some studies have reported potential degradation of certain polymers. Such as discoloration or changes in fiber diameter, during such oxidative digestion (Stanton et al., 2019; Treilles et al., 2020), recent work by Silva et al. (2024) demonstrated that common oxidative pretreatments like H_2O_2, when applied with caution, do not substantially modify the vibrational spectra of most of the targeted polymers, thereby not impeding their chemical identification by Raman spectroscopy. Nevertheless, in the present study we preferred to avoid any chemical digestion altogether in order to minimize the risk of physically altering or losing fragile fibers during sample processing.

Table 1
Summary of collected ice core samples along with their respective information.

Core	T13-K1					
Coordinates	Lat: 43 12.587 Long: 131 50.680					
Sampling date	26/02/2020					
	Thickness cm	Weight g	Volume L	Salinity (ppt)	CDOM	Ch-l
Layer 1	4.1	714.2	0.824	7.46	1.62	0.12
Layer 2	5.2	906.1	1.046	4.81	0.74	0.03
Layer 3	5.3	916.1	1.066	5.43	0.55	0.01
Layer 4	4.8	829.8	0.965	4.84	0.42	0.02
Layer 5	5.0	870.3	1.005	4.40	1.02	0.06
Layer 6	4.9	849.2	0.985	4.60	0.59	0.23
Layer 7	4.1	720.4	0.824	4.33	1.37	0.15
Layer 8	4.7	813.9	0.945	10.89	5.41	3.14
Tot	38.0	6620	7.660			

Core	T15-K4					
Coordinates	Lat: 43 12.968 Long: 131 49.684					
Sampling date	21/02/2020					
	Thickness cm	Weight g	Volume L	Salinity (ppt)	CDOM	Ch-l
Layer 1	4.2	747.5	0.845	6.65	1.44	0.04
Layer 2	5.7	1016.5	1.146	4.76	0.76	0.01
Layer 3	5.1	910	1.026	5.24	0.94	0.02
Layer 4	5.0	902	1.006	5.17	0.81	0.02
Layer 5	5.4	966	1.086	4.88	1.28	0.06
Layer 6	5.5	985	1.106	4.56	2.93	0.13
Layer 7	4.9	878	0.986	3.77	2.81	0.16
Layer 8	4.8	871	0.965	4.21	2.05	0.23
Layer 9	4.4	800	0.885	4.51	2.7	0.47
Layer 10	4.9	885	0.986	9.90	6.81	3.21
Tot	49.8	8961	10.036			

Coordinates	Lat: 43 12.978 Long: 131 49.688					
Cores	T15-K2					
Sampling date		27/02/2020				
	Thickness cm	Weight g	Volume L	Salinity (ppt)	CDOM	Ch-l
Layer 1	3.6	612	0.724	6.67	1.73	0.12
Layer 2	4.9	834.8	0.985	5.22	0.53	0.03
Layer 3	5.2	888.1	1.046	5.16	0.4	0.02
Layer 4	5.2	890.8	1.046	5.08	0.29	0.02
Layer 5	5.4	922.8	1.086	5.38	0.48	0.03
Layer 6	4.7	796	0.945	4.91	1.16	0.06
Layer 7	4.6	786.8	0.925	3.95	1.52	0.16
Layer 8	5.0	845.6	1.005	3.55	1.69	0.25
Layer 9	4.9	828.1	0.985	4.00	2.21	0.23
Layer 10	4.7	795.3	0.945	4.75	4.04	0.34
Layer 11	4.6	782.8	0.925	9.71	9.18	6.39
Tot	52.7	8983.1	10.617			

At present, this methodological variability among studies still limits the comparability of results and the accurate assessment of MF environmental distribution and accumulation zones (Suaria et al., 2020; Ivleva, 2021) and several hypotheses have been proposed regarding the environmental compartments where microplastics and microfibers may preferentially accumulate (Cózar et al., 2014). Among the possible environmental sinks for anthropogenic particulate pollution, sea ice has recently received increasing attention, as it may act as a temporary reservoir for MPs (Peeken et al., 2018; Chubarenko et al., 2022). With ongoing climate change and the progressive melting of sea ice, it has been also envisaged that large quantities of these trapped particles could be reintroduced into the marine environment (Obbard et al., 2014; Chubarenko, 2022). It is reasonable to hypothesize that sea ice may similarly serve as a sink for MFs. However, our current understanding of the occurrence, distribution, and composition of MFs in sea ice remains limited. To date, only about ten studies have addressed the occurrence of MFs in sea ice, and among these, only four employed protocols that did not involve strong acid or oxidative digestion, potentially leading to underestimation of their abundance.

Building upon this premise and with the aim of advancing current knowledge on the occurrence of MPs and MFs in sea ice and their environmental implications, we conducted a field campaign to determine their abundance, chemical composition, and vertical distribution in the seasonal sea ice of Amur Bay (Sea of Japan, Russia). Here, we report and discuss the results obtained from three different ice cores.

2. Materials and methods

2.1. Study area and location of sampling points

The sea-ice object of the present study was collected from the northern part of Amur Bay (Sea of Japan). The map of the study area with the precise location of the sampling points is reported in Fig. 1. The Amur Bay (Russian: АМурский залив, Amursky zaliv) is located in the northwestern part of Peter the Great basin in the Sea of Japan, within 131° 15′-132° 05′ E and 42° 50′-43° 20′ N, and consists of a semi-closed shallow water area of about 966 km^2. Its western boundary is the continental coast, and its eastern boundary is the coastline of the Muravyov-Amursky Peninsula (port of Vladivostok) and the islands extending southwestward from it: Russky, Popov, Reineke, Rikorda, Tsivolko, and Zheltukhina. The bay stretches about 65 km in length, with a width ranging from 9 to 20 km. The Razdolnaya River flows into the northern part of the bay, while the Shmidtovka and Bogataya Rivers enter from the northeast, and the Amba, Barabashevka, and Narva Rivers from the northwest. The bay bottom is an accumulative plain gently sloping toward the sea. Depth gradually increases from 0 to 53 m, with an average of 15 m. A shallow zone up to 5 m deep extends around the head of the bay (1–5 km wide) and along the northwestern coast. The southeastern shore of the bay is mountainous, whereas the western and northern shores are mostly low-lying with sandy beaches. The underwater relief includes a large sublatitudinal ridge (the Muravyov Threshold), rising 8–15 m above the bottom, stretching from the southern tip of the Peschany Peninsula to Russky Island. This ridge causes the accumulation of nearly all the solid load carried by the Razdolnaya River in the northern part of the bay (Gomoyunov, 1927; Petrenko and Manuilov, 1988; Podorvanova et al., 1989; Lotsiya, 1996). The transboundary Razdolnaya River (Chinese: 绥芬河, Suífēnhé) drains a catchment area of 16,830 km^2, of which 6820 km^2 belong to Russia (Ussuriysky, Nadezhdinsky, and Oktyabrsky districts of Primorsky Krai) and about 10,000 km^2 to China (Dongning and Suifenhe counties and Suifenhe City of Mudanjiang Prefecture, Heilongjiang Province, PRC). The river regime is characterized by an average discharge of 103.5 m^3/s (over the last 11 years), with minimum flows in winter (7.2 and 5.7 m^3/s in January and February, respectively). Floods occur in spring (up to 1000

m^3/s in May due to snowmelt) and in summer and autumn (up to 3000 m^3/s following tropical cyclones). The Russian part of the region is densely populated: 634000 inhabitants in the Vladivostok urban district and about 256,000 in settlements along the Razdolnaya River, including Ussuriysk (180000) (as of 2020). In China, the combined population of Dongning and Suifenhe counties does not exceed 280,000 (based on 2003 and 2010 estimates; more recent census data are not publicly available). Local climate is monsoon-driven, with humid sea air and southerly winds in spring and summer, and dry continental air with northerly winds in autumn and winter. Winter typically begins in mid-November and lasts about 130 days. During this period, air temperatures regularly drop below −20 °C due to southward movements of the Siberian High (Talley et al., 2003). Air temperature in winter in the area is about −6 to −16 °C with a mean of around −8.4 °C (Mel'nichenko et al., 2019). The amount of precipitation during the winter season is about 40 mm (from 8 to 80 mm) (https://rp5.ru/). In summer, blowing warm and humid air from the North Pacific. The warmest month is August, when the average air temperature reaches 25 °C or more. The annual precipitation is about 900 mm (https://rp5.ru/). The mean annual surface water temperature in Amur Bay is about 8 °C. Minimum surface temperatures are recorded in February (−1.8 °C or lower, during ice formation), while maximum values occur in August (26 °C or higher). Homothermy is observed in winter (November–March), and a seasonal thermocline develops in summer (June–September) due to surface heating. Because of its geomorphology, Amur Bay is characterized by early freezing and a long ice-covered period lasting 110–130 days. The estuarine part of the bay (including the T-transect stations) is completely ice-covered by late December, with ice melt by mid-March and open waters in April (see Supplementary S1). In winter, salinity is largely controlled by ice formation (brine rejection), while in summer it is influenced by precipitation, river discharge, and inflow from the open sea. The annual salinity trend shows a maximum in February (35.4) and a minimum in July–August (20.4). The tidal regime of the bay is irregular semidiurnal, with amplitudes not exceeding 0.5 m, and tidal currents are weak (2–5 cm/s). The waters of Amur Bay are subject to significant anthropogenic pressure. Agriculture and industrial facilities are developed in the Razdolnaya/Suifun River valley. The bay is characterized by active navigation, and its shores host port facilities, shipyards, an oil depot, and a fish-processing plant. At the same time, a large portion of the coast is used for recreation. Additional sources of pollution in Amur Bay include municipal wastewater from Vladivostok. Deepwater outfalls from wastewater treatment plants are shown in Fig. 1: in the north near the De-Friz Peninsula (N, discharge up to 15,000 m^3/day) and in the central urban area (C, 79000 m^3/day).

2.2. Ice core sampling

The sampling and analytical procedures used in this study closely follow those previously described in Chubarenko et al. (2022), as the three ice cores named T13-K1, T15-K4 and T15-K2 and object of the here presented study were collected from seasonal ice during the same expedition (carried out from January 23 to February 27, 2020) and processed in the same laboratory facilities. More specifically, Ice Core T15-K2 was sampled by February 27 at 10 m from the Ice Core T15-K4 (February 21), while the Ice Core T13-K1 (February 26) was collected approximately 1500 m from the other two. Water depths at the sampling locations were 18.9 m for T13-K1 and 17 m for both T15-K4 and T15-K2. Table 1 reports further including the thicknesses of individual core sections and their corresponding weight and meltwater volumes. To investigate spatial salinity distribution (and CDOM and chlorophyll-a), additional cores were collected from both the T13 and T15 areas. All collected ice cores were cut with a circular drill (internal diameter 16 cm) after snow removal (thickness 5–8 cm) with a metal spatula. After extraction, the total length (ice thickness) of each core was measured with an accuracy of 0.5 cm. Then, the ice cores were wrapped in aluminum foil, sealed into Teflon zip-lock bag plastic bags, and transported to the laboratory, where they were stored horizontally in a laboratory freezer at −18 °C until further processing. Images related to the on-site operation are provided in Supplementary files (see Supplementary S2). The collected ice was then melted in a dark room at a temperature of +22 °C for 24 h. The melted water was then thoroughly mixed according to the method described by Mel'nichenko et al. (2019) and passed through the SBE-19 plus CTD probe flow system, equipped with the main SBE-3 and SBE-4 sensors, as well as WS3S and ECO CDOM WSCD fluorescence. This instrument enables salinity determination accuracy at 0.1, chlorophyll "a" at 0.2 μ g/L and CDOM at 0.2 μ g/L (Supplementary S3).

2.3. MPs extraction

Sample preparation for the extraction of MPs and MFs from the sea ice involved a preliminary sectioning of the collected ice cores similar to those applied for salinity determination, but with adjustment to avoid external contamination. Briefly, the cores were sliced into segments roughly 5 cm thick, starting from the bottom. Each ice slice was then wrapped in aluminum foil and transferred to a 2.4 L glass container. The ice content was then determined by weighting on a Kern EW3000-2 M balance with an accuracy of 0.1 g. After that, the aluminum was removed and the collected ice slices were melted at room temperature. The melted water collected in each bottle was then passed through nitrocellulose filter (diameter 47 mm, pores 0.45 μm, nitrocellulose, MF-Millipore (France) using a dedicated filter unit (Merck, Millipore) preserved in a clean room environment. Filters were then placed in Petri dishes covered with a lid, sealed, labeled (see Supplementary S4) and then shipped to the University of Milan-Bicocca for micro-FTIR analysis.

2.4. μ-FTIR analysis

Analysis of the filters were carried out using a μ-FTIR instrument Spotlight 200i (Perkin Elmer), equipped with a liquid nitrogen cooled mercury cadmium telluride (MCT) single detector. The spectra were collected in reflectance mode, collecting 32 coadded scans for each analysis point, and by applying a scan range of 3600–700 cm^{-1}, resolution of 4 cm^{-1} as described in Saliu et al. (2023). Briefly, to ensure a statistically representative sampling of all the potential MPs and MFs on the filter surface, three image surveys (5 × 5 mm) were acquired for each filter. All visible items (fibers, fragments, films) within each survey area were counted systematically from top to bottom and left to right. Specifically, the items submitted to μ-FTIR analysis were selected on the basis of their size (we analyzed the items between 15 μm and 5000 μm). Items smaller than 15 μm were excluded due to the physical resolution limits of infrared radiation (Kansiz et al., 2020). For each particle, also color and shape features were annotated.

Approximately 20% of the counted items were then analyzed by μ-FTIR. This approach covered approximately 4.5% of each filter's total surface area (considering three technical replicates per filter). This partial survey strategy was adopted due to time constraints, since analyzing the entire 47 mm-diameter filter surface may require up to two weeks and the large variety of items on the chemically untreated filter prevent the application of automated recognition protocols based on unsupervised mapping of the filter surface and deconvolution of the items from the collected spectra by multivariate statistical analysis. Patented COMPARE™ spectral comparison algorithm provided by Perkin Elmer was used to confirm the assignment of the particles by comparison with the reference spectra library (Saliu et al., 2020) (see Supplementary S5). Only matches with a confidence level of 70% or higher were accepted. Background spectra were collected prior to each acquisition.. Notwithstanding the distinct library matches, we categorized all the cellulosic fiber within the same group designed as rayon/cellulose. This approach was selected due to well-documented difficulties in discriminating between these two polymers, particularly when aged or weathered (Lusher et al., 2014; Peeken et al., 2018; Suaria et al.,

2020; Cai et al., 2019; Loof et al., 2016).

2.5. Contamination and quality controls

To mitigate any possible sources of external contamination, we adopted several precaution measures from the sample collection till the sample preparation and analysis. Specifically, during the sampling operation maximum care was taken for excluding any contact between the surface and the snow. During lab operation, clean conditions were kept and the use of plastic material was carefully avoided. Only pre-cleaned stainless tools and glass water were used. The analysis with micro-FTIR were carried out in a Clean Room (standard ISO series 14,644) ISO 6, air changes per hour between 150 and 240 and 293 particles/$m^3 \geq 5$ μm, with proper dressing PPEs (see Supplementary S6). Six procedural blank samples were processed together with the ice core samples for determining background contamination and performing blank substruction. These blanks were obtained by carrying glass bottles previously filled with milliQ water in the sampling location and by processing them following the same procedure applied to the melted ice obtained from the cores. Blank controls were run to evaluate the level of background contamination in order to apply blank subtraction. In addition, clean Petri dishes (90 mm) with paper filters were exposed near working places and the occurrence of plastic and fibers was noted to check for comparable levels of background in the working environment.

2.6. Statistical analysis

All the data collected during the experimental activity were expressed as mean ± standard deviation (SD) (see Supplementary S7). Data normality was assessed using the Shapiro-Wilk test. Since the normality assumption was not met, the non-parametric Kruskal-Wallis test was applied to investigate differences in MPs and MFs abundance between the different ice cores and their respective layers. Values were considered statistically significant at $p < 0.05$. Correlations between MPs and MFs abundance and environmental variables were examined using the non-parametric Spearman rank correlation test. Principal Component Analysis (PCA) was conducted considering each ice core and the layer within the cores as distinct observable and with the aim of better highlighting emerging patterns and relationships between MFs and MPs distribution (expressed as fibers fragments and films per liter) and the other environmental parameters used to characterize sea ice (salinity, CDOM, Ch-l). Given the non-normal distribution of most variables and the relatively small sample size, PCAs were conducted on the Spearman rank correlation matrix. Furthermore, comparisons between Pearson and Spearman correlation coefficients revealed substantial differences for several variable pairs, indicating the presence of non-linear but monotonic relationships. This supported the use of Spearman-based PCA to better capture the underlying structure in the data. All analyses were performed using XLSTAT (XLSTAT, Lumivero, Denver, USA).

3. Results

3.1. MPs and MFs in three ice cores from Amur Bay

The 29 ice slices of 5 cm average thickness obtained from the three ice cores showed ice mass from 714.2 to 1016.6 g (see Table 1), for a total of 24.5 kg of sea ice analyzed and 6026 anthropogenic particles identified. Considering the items' shape 5708 (94.71%) were fibers, 246 (4.08%) were fragments, and 72 (1.20%) were films (see Supplementary S8). Volume-normalized data showed that items with a fibrous shape constituted 97.0%, 94.3%, and 93.6% of the total particles in T13-K1, T15-K4, and T15-K2, respectively. Fragments and films were 1.9% and 1.1% in ice core T13-K1; 3.7% and 2.0% in T15-K4; and 5.1% and 1.3% in T15-K2. The highest abundance of fibers was recorded in layer 11 of

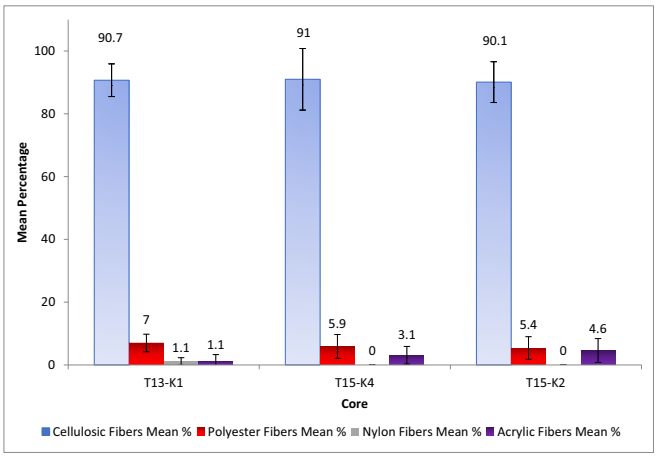

Fig. 2. Mean abundance (%) of fiber polymer type per liter in the three ice cores. Note how the presence of cellulose fibers is clearly predominant compared to the other polymers. Rayon fibers are included within the cellulose fibers.

core T15-K2 (8409 ± 229 fibers per liter, ~ 45 cm depth), while the lowest was in layer 2 of core T15-K4 (947 ± 30 fibers per liter, ~10 cm depth). The greatest number of fragments and films was observed in layer 9 of T15-K2 (832 ± 179 items per liter, ~40 cm depth), while the lowest was in layer 2 of T13-K1 (42 ± 25 items per liter, ~ 10 cm depth). Films showed very low concentration (mean valued 14 items per liter), with 6 out of 29 layers resulting with no films detected (see Supplementary S9).

Considering the chemical composition, 750 fibers of the 774 fibers detected, yielded a positive match with the reference library (Fig. 2). More specifically, in the ice core T13-K1, 238 fibers were characterized, of which 90.34% were rayon/cellulose, 7.14% polyester, 2.10% acrylic, and 0.42% nylon. In the core T15-K4, 215 fibers were characterized, of which 92.09% were rayon/cellulose, 6.05% polyester, 1.86% acrylic, and no nylon was detected. In the core T15-K2, 297 fibers were analyzed, of which 90.57% were rayon/cellulose, 4.71% polyester, 4.71% acrylic, and again, no nylon fibers were found.

Overall, 682 (90.93%) of the 750 analyzed fibers were cellulose-based (see Supplementary S10).

Among fragments and films, the most frequently identified polymers were cellulose nitrate (20%), polyethylene (16%), polystyrene (12%), and cellulose acetate (12%). A comprehensive list of all identified polymers for fragments and films is provided in Supplementary S11.

The bulk mean (volume-weighted mean) of items per liter (fibers, fragments, and films) in Core T13-K1 is 5109 ± 1510 items/L, with a fibers-to-nonfibers ratio of 33:1. Core T15-K4 has a bulk mean of 2009 ± 581 items/L and a fibers-to-nonfibers ratio of 17:1. Core T15-K2 shows a bulk mean of 6992 ± 1614 items/L, with a fibers-to-nonfibers ratio of 14:1. The sum of these values yields a total bulk mean of approximately 4716 ± 2509 items/L, with fibers accounting for about 94% of the total (see Table 2).

When excluding cellulosic fibers, the bulk mean for Core T13-K1 decreases to 599 ± 93 items/L, with a fibers-to-nonfibers ratio of 3:1. In this core, synthetic MFs account for approximately 75% of the total items. In Core T15-K4, the bulk mean drops to 270 ± 143 items/L, with a fibers-to-nonfibers ratio of 1.4:1, and MFs represent about 58% of the total items. Core T15-K2 shows a decrease to 1139 ± 638 items/L, with a fibers-to-nonfibers ratio of 1.5:1, where MFs account for approximately 60.5% of the items. Overall, this corresponds to a total bulk mean of approximately 685 ± 550 items/L, with synthetic fibers contributing to about 64.5% of the total (see Supplementary S12).

Considering the sizes, most of the detected items were in the range 0.3–3 mm. More specifically, 81.7% of items in core T13-K1, 86.2% in core T15-K4 and 77,4% in core T15-K2. Items smaller than 0.1–0.3 mm

Table 2
Results of the MFs and Mps characterization of the Amur Bay ice cores, including bulk mean values (items/L) for fibers, fragments, and films, and the overall fiber-to-fragment/film ratio. Standard deviations (SD) reported for each layer are calculated from three replicate counts conducted on 5 × 5 mm areas of the filter (representing ~4.5% of the total surface). The SD associated with the bulk mean is computed across all layers of the ice core and reflects the inter-layer variability of MFs and fragment/film abundances.

T13-K1	Fibers per liter	Fragments/film per liter	Total by layer	Fibers/ fragments-films ratio
Layer 1	4301 ± 262	161 ± 41	4462 ± 262	26.7
Layer 2	4260 ± 77	42 ± 25	4303 ± 111	100.5
Layer 3	3286 ± 375	166 ± 43	3452 ± 183	19.8
Layer 4	3031 ± 144	92 ± 0	3123 ± 60	33.0
Layer 5	5070 ± 122	132 ± 0	5202 ± 272	38.3
Layer 6	7310 ± 432	225 ± 39	7535 ± 204	32.5
Layer 7	6694 ± 118	188 ± 16	6882 ± 41	35.6
Layer 8	6074 ± 176	211 ± 24	6285 ± 81	28.8
Bulk Mean		5109 ± 1510		
Total ratio				33

T15-K4	Fibers per liter	Fragments/film per liter	Total by layer	Fibers/ fragments-films ratio
Layer 1	1653 ± 95	131 ± 15	1784 ± 144	12.6
Layer 2	947 ± 30	58 ± 34	1005 ± 34	16.3
Layer 3	2700 ± 218	194 ± 0	2895 ± 254	13.9
Layer 4	1785 ± 138	198 ± 0	1983 ± 92	9.0
Layer 5	1857 ± 63	20 ± 12	1877 ± 43	91.0
Layer 6	2684 ± 191	120 ± 31	2805 ± 303	22.3
Layer 7	2518 ± 181	90 ± 23	2608 ± 179	28.0
Layer 8	1722 ± 46	138 ± 13	1859 ± 85	12.5
Layer 9	1628 ± 63	75 ± 14	1703 ± 49	21.7
Layer 10	1439 ± 34	112 ± 23	1552 ± 77	12.8
Bulk Mean		2009 ± 581		
Total ratio				17

T15-K2	Fibers per liter	Fragments/film per liter	Total by layer	Fibers/ fragments-films ratio
Layer 1	6152 ± 276	61 ± 18	6213 ± 277	100.5
Layer 2	4522 ± 1109	382 ± 26	4904 ± 1109	11.8
Layer 3	7902 ± 318	318 ± 21	8220 ± 319	24.9
Layer 4	5974 ± 216	191 ± 0	6165 ± 216	31.3
Layer 5	3448 ± 515	265 ± 63	3741 ± 519	13.0
Layer 6	7692 ± 130	234 ± 41	7926 ± 136	32.8
Layer 7	6971 ± 208	599 ± 83	7570 ± 224	11.6
Layer 8	7916 ± 166	441 ± 13	8357 ± 167	18.0
Layer 9	5939 ± 373	832 ± 179	6772 ± 414	7.1
Layer 10	7410 ± 516	797 ± 130	8207 ± 532	9.3
Layer 11	8409 ± 229	791 ± 37	9199 ± 232	10.6
Bulk Mean		6992 ± 1614		
Total ratio				14

range and in the 3–5 mm range, represented significantly smaller fractions in all cores (see Supplementary S13). We did not detect any MPs and MFs in the <0.1 range.

In terms of MFs color, we observed five predominant colors: transparent/white (75.6% in core T13-K1, 77.8% in core T15-K4, 79.1% in core T15-K2), blue (16.8% in core T13-K1, 16.1% in core T15-K4, 17.8% in core T15-K2) red (5.9% in core T13-K1, 4.4% in core T15-K4, 3.0% in core T15-K2). Purple (0.8% in core T13-K1, 1.1% in core T15-K4, absent in core T15-K2) and orange (0.8% in core T13-K1, 0.6% in core T15-K4, absent in core T15-K2). In fragments and films, 7 colors were identified: brown (25%), white (22%), yellow (19%), blue (13%), green (9%), red (6%), light blue (6%). More details regarding color distribution are available in the Supplementary (S14).

3.2. Statistical analysis

Kruskal-Wallis test carried out considering the distribution of the different items detected in the different ice cores and ice layers showed the occurrence of a significant difference between the three cores for MFs abundances per liter (p-value = 0.00003, $\alpha = 0.05$). More specifically, the post-hoc pairwise comparisons (Dunn's test with Bonferroni correction) revealed a significant difference between T13-K1 and T15-K4 (p-value = 0.010, $\alpha = 0.05$), and a significant difference between T15-K4 and T15-K2 (p-value = 0.004, $\alpha = 0.05$), while no significant difference was observed between T13-K1 and T15-K2 (p-value = 0.150, $\alpha = 0.05$). A statistically significant difference was also highlighted by considering the MFs distribution within the layers of core T15-K4 (p-value = 0.038, $\alpha = 0.05$). More specifically, the MFs abundance in the middle layer (expressed as MFs per liter) was statistically different from the top (first 10 cm) and the bottom (last 10 cm). Differently, no significant differences were highlighted for the distribution in the core T13-K1 (p-value = 0.4, $\alpha = 0.05$) and T15-K2 (p-value = 0.248 $\alpha = 0.05$). More details related to the observed distributions are reported in Fig. 3, and Supplementary S15.

In Fig. 4 the Biplots obtained by applying Principal Component Analysis (PCA) to the data representing MFs distribution along the different layers within the three different ice core are reported. The corresponding Spearman correlation matrixes are shown in Table 4. In core T13-K1, the PCA explained 84.28% of the total variance. PC1 was primarily driven by Ch-l (31%), fibers per liter (30%), and fragments/films per liter (22%), while PC2 was dominated by salinity (76%) and CDOM (15%). A cluster determined by values close to zero or slightly negative along PC1 is observed. In addition, the occurrence of an outlier is clearly highlighted, in this core as in the other two cores. In all the cases the outlier corresponds to the bottommost layer (the layer that is in contact with seawater). This layer is characterized by elevated levels of salinity, CDOM, and Ch-l, which are not observed in the other layers. Considering the correlation matrix, a strong positive correlation was observed between fiber and fragment abundances (Spearman's $\rho = 0.762$, $\alpha = 0.05$), and both were also positively associated with Ch-l ($\rho = 0.881$, $\alpha = 0.05$) and CDOM ($\rho = 0.524$, $\alpha = 0.05$). In contrast, salinity showed a moderate negative correlation with fiber abundance ($\rho = -0.381$, $\alpha = 0.05$). In T15-K4, the PCA explained 67.27% of the variance. PC1 was mainly influenced by CDOM (38%) and Ch-l (43%), while PC2 was driven by fibers (56%) and fragments/films (35%). Correlation analysis revealed a moderate positive association between fibers and fragments ($\rho = 0.358$, $\alpha = 0.05$), while no clear correlation was found with environmental parameters. Interestingly, salinity showed weak and negative or negligible correlations with all variables. In core T15-K2, the explained variance was 77.54%. PC1 included contributions from CDOM (29%), Ch-l (33%), and fragments/films per liter (24%), while PC2 was largely dominated by salinity (74%). Fiber abundance showed only weak to moderate positive correlations with CDOM ($\rho = 0.373$, $\alpha = 0.05$) and chlorophyll-a ($\rho = 0.466$, $\alpha = 0.05$), and a negative correlation with salinity ($\rho = -0.127$, $\alpha = 0.05$). A moderate correlation was observed between fragments/films and both CDOM ($\rho = 0.636$, $\alpha = 0.05$) and Ch-l ($\rho = 0.699$, $\alpha = 0.05$), suggesting partial co-distribution. Considering the relationship between cellulosic and synthetic fibers, a negative correlation in T13-K1 ($\rho = -0.429$, $\alpha = 0.05$) and T15-K4 ($\rho = -0.333$, $\alpha = 0.05$) was observe, while no correlation was found in the ice core T15-K2 ($\rho = -0.027$, $\alpha = 0.05$). Finally, synthetic fibers showed a moderate to strong positive correlation with salinity in T13-K1 ($\rho = 0.357$, $\alpha = 0.05$) and T15-K4 ($\rho = 0.515$, $\alpha = 0.05$), but a strong negative

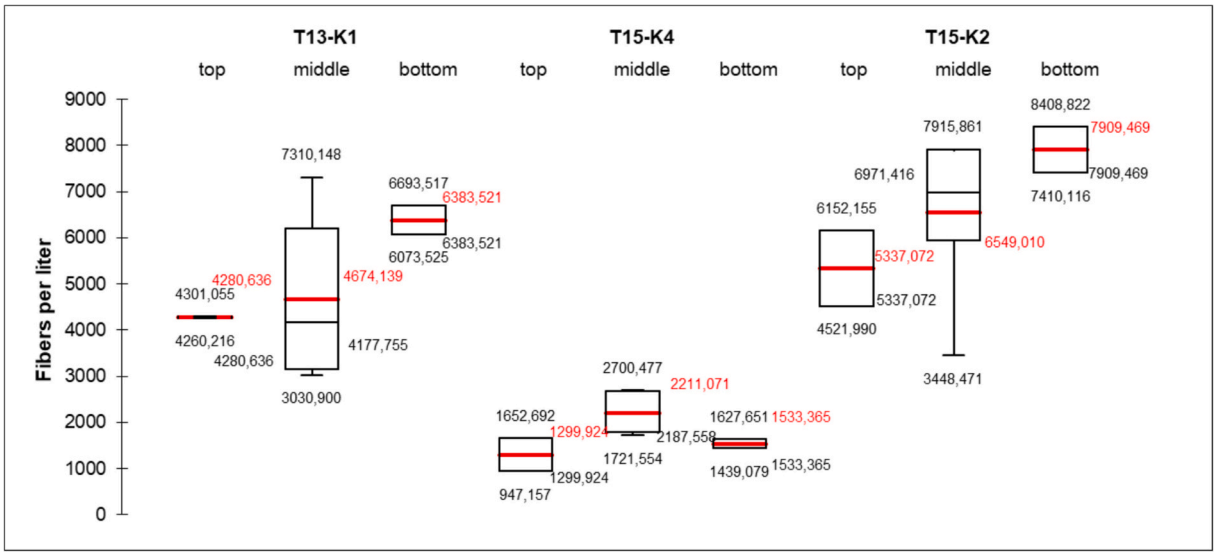

Fig. 3. Boxplot showing fibers distribution across the top (first 10 cm), middle (between top and bottom), and bottom (last 10 cm) layers of each ice core. A significant difference was observed between core T15-K4 and the other two cores, as revealed by the Kruskal-Wallis test. No significant differences were found in fibers' abundance within each individual core, except for core T15-K4, where a significant difference was observed. Red line within the boxes indicates the mean, meanwhile black line the median. (For interpretation of the references to color in this figure legend, the reader is referred to the web version of this article.)

correlation in T15-K2 ($\rho = -0.788$, $\alpha = 0.05$), see Supplementary S16 for PCA and Spearman correlation matrix.

4. Discussion

4.1. Occurrence of anthropogenic items in the sea-ice of Amur Bay: comparison with previous literature data and possible local environmental and anthropogenic factors to be considered

As reported in the Results section, the first-year sea ice of Amur Bay contained a high abundance of anthropogenic items, with concentrations ranging from 6992 ± 1614 items/L to 2009 ± 581 items/L. The majority of these particles were microfibers (MFs), which accounted for approximately 97% of the total items detected. While the prevalence of MFs in subsurface seawater, rivers, and the atmosphere has already been documented in several studies (see the Introduction section of this paper), this finding can be considered unprecedented for sea ice. Indeed, reports concerning the occurrence of cellulosic MFs in sea ice remain very limited. To the best of our knowledge, only four studies have reported data on MF abundance in sea ice (see Table 3), and among them, only one included cellulosic fibers in the counts (Friesen et al., 2020).

Overall, these previous studies display large variability in the relative abundance of fibers, both in terms of their proportion compared to films and fragments - 79% in Kanhai et al. (2020), 84% in Kim et al. (2021), 39% in Friesen et al. (2020), and 38% in Chubarenko et al. (2022) - and in their absolute concentrations, which vary over several orders of magnitude. Such discrepancies may not necessarily reflect real differences in contamination levels but could rather arise from methodological variability among studies. Differences in sampling strategies, ice melting procedures, and particle isolation and identification techniques can strongly influence the reported abundances (see Introduction, paragraph on the influence of sampling and processing methods).

For instance, Kelly et al. (2020) reported land-fast sea ice from East Antarctica for abundance values related to MPs and MFs from 6 to 33.3 particles per liter (mean: 20.38 particles/L). These values were obtained by analyzing a single archived core collected 12 km north of Casey Station. A total of 96 MPs particles were identified using μFTIR, with sizes ranging from 20 to 325 μm (mean: 56.7 μm). Two sample processing methods were tested: one including a chemical oxidation step with hydrogen peroxide (H_2O_2) and one involving prefiltration through 5 μm filters to reduce biomass. Both approaches included H_2O_2 treatment before analysis. A total of 14 polymer types were identified, of which rayon and wool fibers accounted for 2% (1% each) of the total particles. The abundances reported in this study are approximately 1.5 to 2 orders of magnitude lower than those observed in our study. However, it should be noted that excluding cellulosic fibers from our dataset reduces the overall bulk mean by nearly one order of magnitude. Specifically, the bulk mean for Core T13-K1 was 599 ± 93 items/L, with fibers accounting for 75% of the total. For Core T15-K4, the value decreased to 270 ± 143 items/L, with fibers representing 58%, while Core T15-K2 yielded 1139 ± 638 items/L, with microfibers comprising about 60.5% of the total. Altogether, this corresponds to an overall bulk mean of approximately 685 ± 550 items/L, with fibers contributing around 64.5%. Therefore, when cellulosic fibers are excluded, our results become broadly comparable to those reported by Kelly et al. (2020), suggesting that the inclusion or exclusion of natural and semi-synthetic fibers can substantially influence the reported levels of microfiber contamination in sea ice.

Obbard et al. (2014) reported an anthropogenic item abundance of 38 ÷ 234 per liter in the multiyear sea ice of Central Arctic, with rayon accounting for 54% of the total MPs found. Four ice cores were analyzed. No chemical treatment was applied to the samples before analysis. This is around >1.5 orders of magnitude lower than in the sea ice obtained in this study. However, the study did not indicate the percentage of MFs compared to the other items considered MPs so we cannot provide a comparison with our data in this respect. Friesen et al. (2020), as already mentioned, focused also on MFs, and analyzed three ice cores from the summer sea ice-edge north of Svalbard without applying any chemical treatment before micro-FTIR analysis (thus applying a protocol very close to the protocol adopted in our study). Among 1597 potential anthropogenic particles, 35 were FTIR-analyzed and ~23% identified as cellulose fibers. The anthropogenic items abundance resulted in 158 ± 155 particles per liter. This is around 1.5 orders of magnitude lower than in the sea ice obtained in this study. In Friesen et al. (2020) study the total fibers represent 39% of the total items found. Ohno et al. (2024) reported an anthropogenic item abundance of 0–60 particles per liter in the fast ice of the Sea of Okhotsk (Shiretoko Peninsula), increasing to 6–263 when including cellulose particles. Four ice cores were retrieved and analyzed; the samples were treated with 30% hydrogen peroxide (H_2O_2) to remove organic matter before micro-FTIR analysis. Only

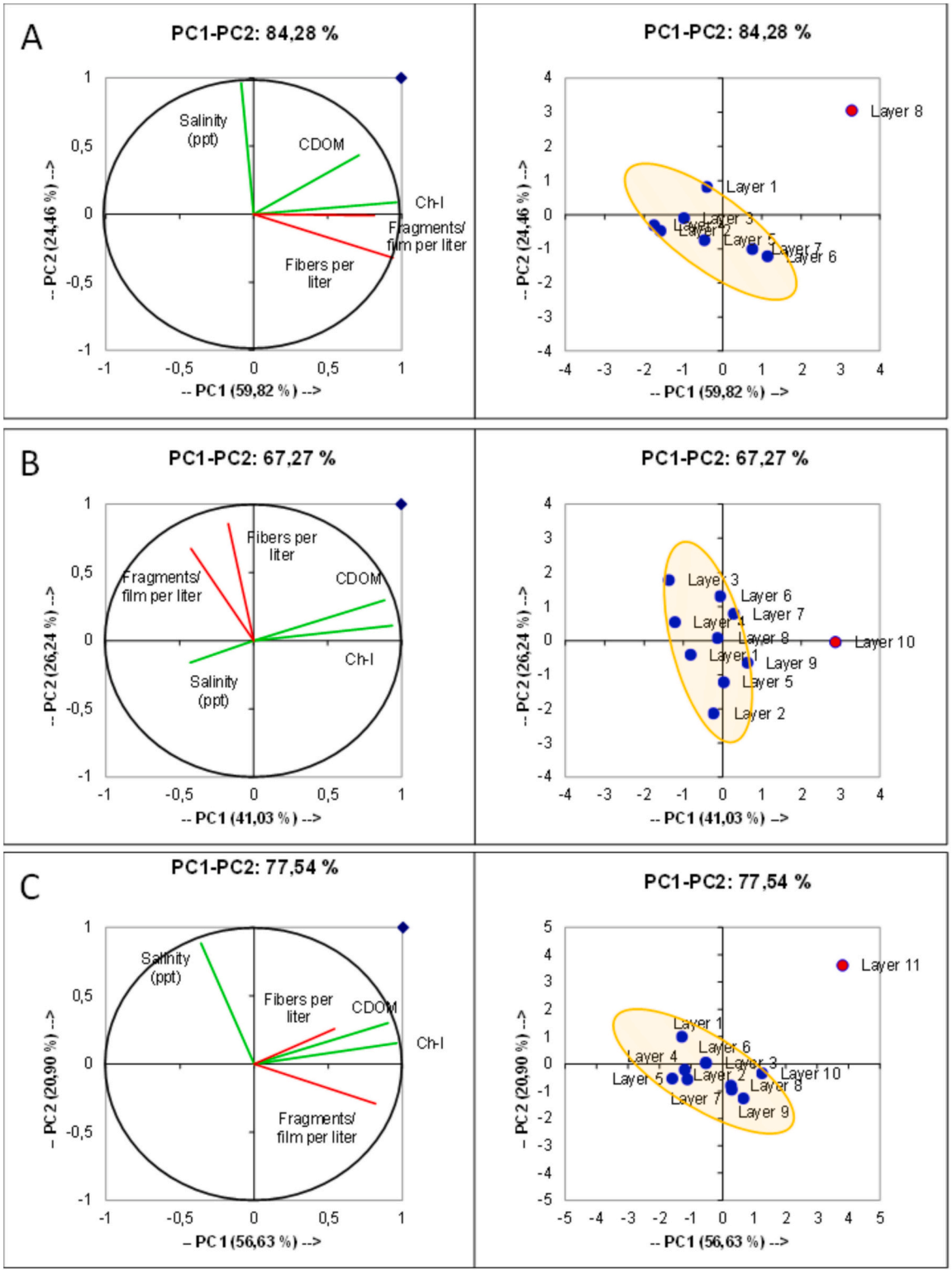

Fig. 4. Principal Component Analysis (PCA) of ice core samples. (A) Core T13-K1: Explained variance: 84.28%. Variable contributions: PC1 - Ch-l (31%), Fibers per liter (30%), Fragments/Films per liter (22%). PC2 - Salinity (76%), CDOM (15%) (B) Core T15-K4: Explained variance: 67,27%. Variable contributions: PC1 - CDOM (38%), Ch-l (43%); PC2 - Fibers per liter (56%), Fragments/Films per liter (35%). (C) Core T15-K2: Explained variance: 77.54%. Variable contributions: PC1 – CDOM (29%), Ch-l (33%), Fragments/Films per liter (24%).; PC2 - Salinity (74%). Outliers are shown in red dots. (For interpretation of the references to color in this figure legend, the reader is referred to the web version of this article.)

particles >30 μm were considered. This is around 1.5 orders of magnitude lower than in the sea ice obtained in this study. (The study does not indicate the percentage of MFs compared to the other items considered MPs). Additionally, Chubarenko et al. (2022) reported a bulk mean of 428 items/L in the first-year sea ice of the Novik Bay (~20 km from our study site), which is around one order of magnitude lower than the abundance observed in this study. However, in this previous study cellulosic fibers were excluded from analysis. When we similarly exclude

Table 3
Comparison of literature data with the data reported in the current study.

Location	Ice type	Size range MPs type specification	Abundance, bulk mean, items/L (% of fibers if included)	Chemically treated (e.g. H_2O_2)	Reference
Central Arctic	Multiyear Ice	<5 mm includes rayon and fibers	38 ÷ 234	No	Obbard et al., 2014.
Fram Strait Nansen Basin North of Svalbard	Pack Ice	11 μm–5 mm excluding fibers, cellulose, rayon	12,000 ± 14,000 2900 ± 2400 2400 ± 1000 1100 ± 800	Yes	Peeken et al., 2018
Fram Strait	Landfast ice	11 μm–5 mm excluding fibers, cellulose, rayon	4100 ± 2000	Yes	Peeken et al., 2018
Gulf of Bothnia, the Baltic Sea	Landfast ice in brackish waters	<5 mm, Nile red detection, no fibers, no rayon-cellulose	8–41	Yes (Nile Red)	Geilfus et al., 2019
Central Arctic	Multiyear ice	<5 mm excluding rayon and cellulose fibers	2–17 (79%)	No	Kanhai et al., 2020
North of Svalbard	Summer sea ice-edge	50 μm–5 mm anthropogenic microparticles including MPs include cellulosic and wool fibers, paints	158 ± 155 (39%)	No	Friesen et al., 2020
Casey Station East Antarctica	Land-fast sea ice	20 μm a 325 μm including cellulose	20.38	Yes	Kelly et al., 2020
Chukchi Sea	Ice floes	>100 μm >20 μm excluding Rayon	11.4 ± 9.12 43.2 ± 32.0 (84%)	No Yes	Kim et al., 2021
Novik Bay, Sea of Japan	First-year ice	25 μm–5 mm excluding cellulose, synthetic dyes	Bulk mean 428 (38%)	No	Chubarenko et al., 2022
Sea of Okhotsk	Fast Ice	>30 μm synthetic >30 μm rayon and cellulosic fibers	0–60 6–263	Yes	Ohno et al., 2024
Amur Bay, Sea of Japan	First-year ice	25 μm–5 mm including rayon, cellulose 25 μm–5 mm excluding rayon, cellulose	Bulk mean 4716 ± 2509 (94%) Bulk mean 685 ± 550 (64,5%)	No	This work

Table 4
Spearman correlation matrix for Core T13-K1, T15-K4 and T15-K2. In bold, statistically significant values (except for the diagonal) at alpha = 0.050 (two-tailed test).

T13-K1	Salinity (ppt)	CDOM	Ch-l	Fibers per liter	Fragments/film per liter
Salinity (ppt)	1	0.214	0.000	−0.381	0.048
CDOM	0.214	1	0.714	0.524	0.310
Ch-l	0.000	0.714	1	0.881	0.714
Fibers per liter	−0.381	0.524	0.881	1	0.762
Fragments/film per liter	0.048	0.310	0.714	0.762	1

T15-K4	Salinity (ppt)	CDOM	Ch-l	Fibers per liter	Fragments/film per liter
Salinity (ppt)	1	−0.164	−0.243	−0.176	0.261
CDOM	−0.164	1	0.875	0.055	−0.115
Ch-l	−0.243	0.875	1	−0.164	−0.182
Fibers per liter	−0.176	0.055	−0.164	1	0.358
Fragments/film per liter	0.261	−0.115	−0.182	0.358	1

T15-K2	Salinity (ppt)	CDOM	Ch-l	Fibers per liter	Fragments/film per liter
Salinity (ppt)	1	−0.045	−0.219	−0.127	−0.409
CDOM	−0.045	1	0.950	0.373	0.636
Ch-l	−0.219	0.950	1	0.466	0.699
Fibers per liter	−0.127	0.373	0.466	1	0.200
Fragments/film per liter	−0.409	0.636	0.699	0.200	1

them, our values become comparable.

Considering the local environmental factors, it must be noted that the ice analyzed in this study is a first-year sea ice, which is formed over approximately three months, from autumn to spring, under inherently variable environmental conditions and a strong influence of river discharge. This suggests that the formation of ice occurs under fluctuating chemo-physical properties such as permeability, porosity, salinity, with different geometry and size of brine channels, and also with possible patchy contamination patterns (e.g., Galley et al., 2015). It is widely reported that young sea ice contains gas and liquid inclusions whose morphology changes over time and depends on atmospheric and oceanic conditions, as well as on whether melting processes have affected the ice (Galley et al., 2015). In spring, sea ice becomes significantly more permeable ("rule of five": at −5 °C and 5 psu, brine pockets coalesce into channels; see Golden et al., 2007). Under such conditions, small contaminant particles may be redistributed via brine channels, while larger particles are more likely to remain frozen in place (Chubarenko et al., 2022). Both upward and downward movement of particles can occur, facilitated by brine drainage or gas bubbles. However, these processes depend on the connectivity and diameter of brine channels, which vary in time and space and cannot be predicted in advance (Chubarenko et al., 2022). More deeply, considering that the cores analyzed in the presented study are from one-year late-winter time ice, the distribution observed might be different for those observed in less permeable winter-time ice or multi-year high-latitude ice (with much smaller gas bubbles and brine pockets, e.g., of about 40 μm in diameters (Callaghan and Eccles, 1996)). General structure of one-year young ice is quite typical: the granular ice of the upper layer is followed by columnar sea ice, and the lower part of the core contains a brine drainage channel structure (e.g., Galley et al., 2015; Mel'nichenko et al., 2019). Particles can become trapped in the ice either from the top (atmospheric deposition) or from the bottom (incorporation during freezing of seawater) (e.g., Dethleff et al., 2009; Chubarenko et al., 2022). Also, local meteorological factors should be included in the dissertation. Between 21 and 27 February (i.e., between sampling of T15-K4 and T15-K2), warming and then heavy-snowing and strong wind happened in the area.

Noteworthy, in all the cores analyzed in the here presented study, the uppermost layers were visibly contaminated by wind-blown coal dust (see Supplementary S17). FTIR analysis confirmed absorption peaks corresponding to hydroxyl (3430 cm^{-1}), aromatic C—H (3055 cm^{-1}), ammonium ion (3242 cm^{-1}), aliphatic C—H (2925 and 2857 cm^{-1}), C═C (1631 cm^{-1}), C—H bending (1435 cm^{-1}), and C—O (1055 cm^{-1}) functional groups. These features are consistent with those previously reported in airborne particulate matter from various combustion sources (Baitimirova et al., 2013). The use of coal for domestic heating is a

known source of this contamination in the area (e.g., Lebedev et al., 2017). Despite the occurrence of this airborne contamination, it was possible to estimate also for these layers the MPs and MFs abundance and it resulted that the surface ice did not show statistically significant different abundances compared to deeper layers. Similarly, the relative abundance of fibers versus fragments/films was not markedly different from that observed in the central and bottom portions of the ice cores. Thus, although the surface was visually impacted by atmospheric deposition, this did not significantly alter the overall distribution pattern of MPs and MFs within the ice column. This suggests their presence can be also related to their occurrence in seawater before the ice formation process and that the items detected throughout the ice columns originate mostly from underlying seawater, transported both horizontally and vertically during ice formation. Moreover, no distinct shift in polymer type or particle category was observed between the uppermost and lower filters, supporting again the conclusion that airborne deposition was not the primary source of contamination. On the other hand, still the particle counts from the surface layers should be interpreted with caution, since their composition may still reflect in part the effect of windborne deposition rather than processes associated with ice formation.

Considering the potential sources of the detected particles, the chemical composition of the fibers revealed the presence of four major polymer types: rayon/cellulose, polyester, nylon, and acrylic. Among these, rayon/cellulose and polyester were predominant. These materials are widely employed in the manufacture of everyday consumer products, particularly within the textile sector. As already noted, we detected a relative abundance of cellulose-based fibers that is substantially higher than that reported in most of the previous research regarding sea ice contamination, including Obbard et al. (2014), Kelly et al. (2020), Friesen et al. (2020), and Ohno et al. (2024).

One possible explanation for this discrepancy lies in the different sample treatment applied, probably more than the local factors related to sampling locations, and ice type. For instance, Kelly et al. (2020) and Ohno et al. (2024) applied hydrogen peroxide digestion prior to chemical analysis, and this harsh chemical approach may dissolve cellulose and rayon-based fibers and even partially degraded polyester (Chubarenko et al., 2022; Silva et al., 2024). In the case of the studies of Obbard et al. (2014) that analyzed multiyear sea ice, and Friesen et al. (2020) that investigated summer sea ice at the northern Svalbard ice edge, local environmental factor and the remoteness of the area might be considered an addition factor to comment the low levels detected of cellulosic fibers in comparison to those we found in the first-year sea ice in Amur Bay, which is in fact closer to urban sources. Unfortunately, most previous studies did not account for the occurrence of cellulosic fibers at all (see, e.g., Peeken et al., 2018; Geilfus et al., 2019; Kanhai et al., 2020; Kim et al., 2021; Chubarenko et al., 2022), and as a result, we should state that the reference data for a detailed comparison are still lacking.

4.2. MFs and MPs size distribution within sea ice

In this study, all the detected particles were categorized into two size classes: small (<0.3 mm) and large (0.3–5 mm), following the same approach previously described in Chubarenko et al. (2022). Particles in the 0.3–5 mm range accounted for more than 84%, whereas particles smaller than 0.3 mm for 16% with the large part of that in the 0.1–0.3 mm range, while smaller sizes were rarely detected (<1%). Interestingly, the small abundance of the smallest size fraction was also reported by Chubarenko et al. (2022) and linked to the high permeability of spring sea ice, where brine channels typically measure about 1 mm and less in diameter (Krembs et al., 2000). In this sea ice, the reduced abundance of particles <300 μm may be explained by a selective removal through brine leakage: MPs and MFs of different sizes accumulate, or are expelled, from sea ice differently. In this context, the observed drop in particle abundance between 150 and 300 μm, also highlighted by Chubarenko et al. (2022), may reflect the occurrence of this size-selective processes. Comparison with theoretical fragmentation models further supports this interpretation, since for both non-fiber particles (mainly fragments) and fibers the power-law distribution is consistent with the related fragmentation model. However, the abundance of fibers sharply decreases below 300 μm, suggesting that smaller fibers are affected by a selection process, probably consisting in a removal during brine migration.

While selective removal through brine drainage offers a compelling explanation for the decline in particles <300 μm, it may not fully account for the near-absence of particles in the 20–100 μm size range. Several complementary factors likely contribute to this observation. First, theoretical models suggest that the production of very small fragments is energetically constrained, as the large energy required to generate particles below a certain size occurs more rarely under natural environmental conditions (Aoki and Furue, 2021). Second, physical mechanisms during ice formation may impose a lower retention limit: particles substantially smaller than typical brine channel diameters could be more efficiently flushed out during brine drainage, particularly if they do not adhere to channel walls (Krembs et al., 2000; Chubarenko et al., 2022). Third, methodological factors cannot be discounted, including potential undersampling of the smallest size fractions due to the partial filter coverage strategy (~4.5% of filter area) and the absence of chemical digestion, which may have resulted in small particles being obscured by residual organic matter. Finally, biological uptake by ice-associated organisms thriving within brine channels may actively remove particles in the 20–100 μm range (Cózar et al., 2014). Future studies employing targeted analytical approaches for small microplastics (<100 μm) would help disentangle these contributing factors.

Another interesting feature is the prevalence of polymers (both for MPs and MFs) whose densities are larger than the density of seawater. This can be considered a clear sign of the very complex hydro physical conditions that affect the growing ice and underneath seawater, under the influence of strong thermo-haline convection and the motion of MFs and MPs (Khatmullina and Chubarenko, 2021). These conditions have been linked to the formation and attachment of gas bubbles, a process that intensifies as water salinity increases (Chubarenko et al., 2023).

4.3. Relevant patterns of MFs and MPs in the three ice core analyzed

As reported in the Results section, the statistical analyses revealed clear differences in the distribution of MPs and MFs among the three ice cores. More specifically, ice core T15-K4 showed a distinct vertical stratification, with the middle layers being the most contaminated. Overall, this core was also the least contaminated, with total abundances approximately two to three times lower than in the other two cores. In contrast, cores T13-K1 and T15-K2 displayed no significant vertical distribution, although both showed a weak increasing trend in particle abundance from top to bottom. These findings suggest the occurrence of localized layering effects, likely influenced by differences in ice formation processes, microstructural properties (granular vs. columnar ice), or by the patchy distribution of particulate matter near the river mouth. The fact that two cores (T15-K2 & T15-K4) were collected only 10 m apart, yet six days apart, further supports the role of short-term variability and dynamic ice growth conditions. Principal Component Analysis (PCA) further highlighted differences in the relationships between environmental parameters and MP/MF distributions. In cores T13-K1 and T15-K4, fibers and fragments/films were positively correlated with CDOM and chlorophyll-a, whereas these associations were weak or absent in T15-K2. Synthetic fibers correlated positively with salinity in T13-K1 and T15-K4, but negatively in T15-K2, possibly reflecting different retention or input mechanisms in each sampling site.

As widely reported in the literature, the potential sources of MFs in the region are multiple. One of the main inputs is domestic laundry, which can release over 1900 fibers per wash from a single garment (Browne et al., 2011; Gago et al., 2018; De Falco et al., 2018; Periyasamy

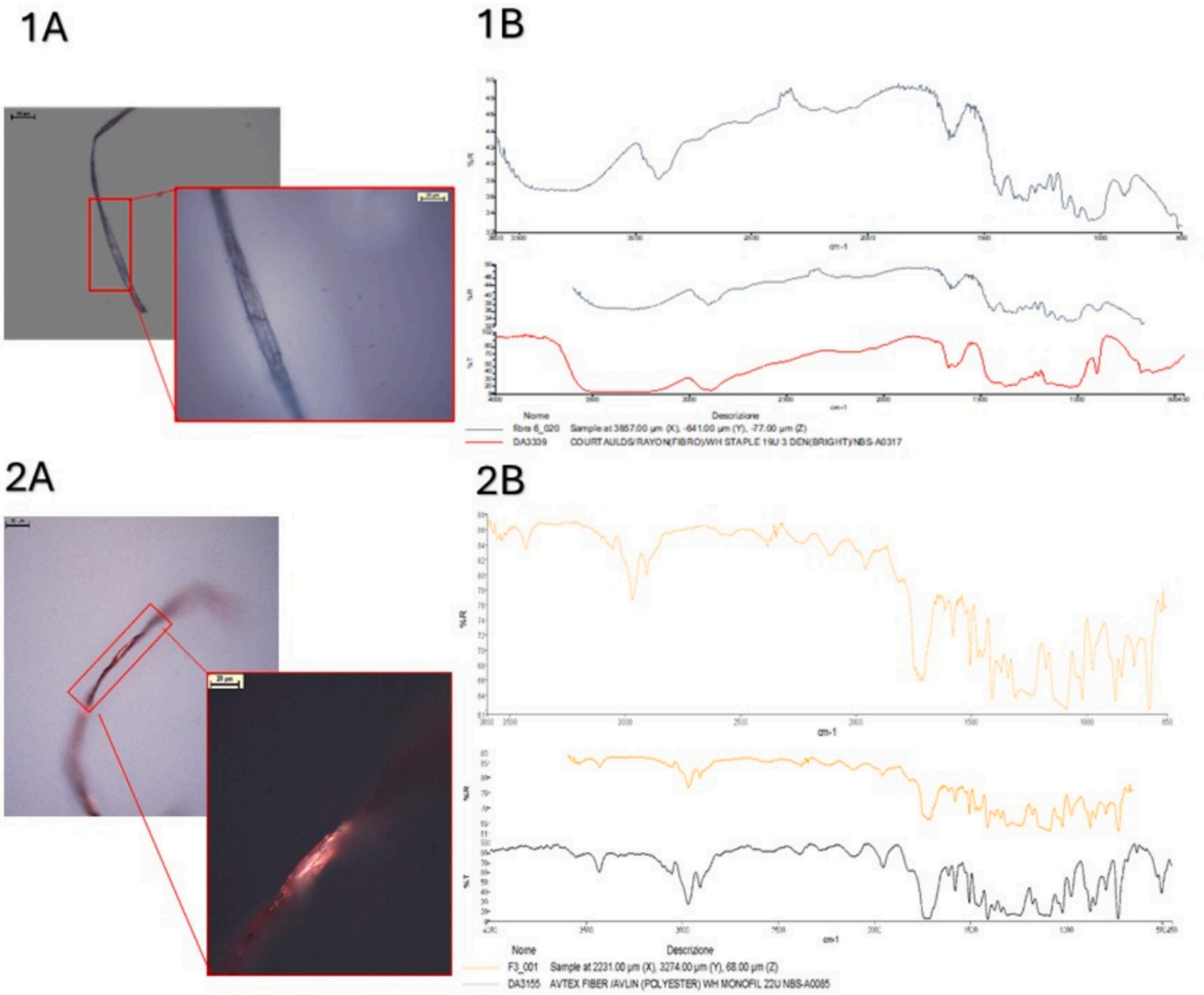

Fig. 5. Representative images of microfibers isolated in this study. (1A) Blue fiber at 200× and 500× magnification; (1B) reference spectrum and library match identified as Rayon. (2A) Red fiber at 200× and 500× magnification; (2B) reference spectrum and library match identified as Polyester. (For interpretation of the references to color in this figure legend, the reader is referred to the web version of this article.)

and Tehrani-Bagha, 2022), with wastewater concentrations exceeding 100 fibers/L. Even after treatment, up to 5% of these fibers may escape from wastewater treatment plants (WWTPs) and be discharged into aquatic environments (Napper and Thompson, 2016; Primpke et al., 2019). Additional pathways include the dispersal of contaminated sludge and atmospheric fallout, as airborne MFs are increasingly recognized as contributors to atmospheric pollution, especially in urban and industrial areas (Dris et al., 2016). All these factors should also be accounted for the observed heterogeneity in MFs distribution.

Insights into the potential origin of MPs can be inferred from their polymer composition. The identified particles were dominated by polymers typically associated with textile materials, namely polyester (47%) and acrylic (25%). This suggests that a significant portion of these fragments may originate from the mechanical fragmentation and weathering of textile products (Napper and Thompson, 2016; Primpke et al., 2019). Conventional packaging-related plastics such as polyethylene (4%) and polystyrene (3%) were also detected, likely deriving from the fragmentation of larger plastic debris and single-use items (Weinstein et al., 2016; Song et al., 2017). The occurrence of polymers such as PTFE (1.0%), epoxy resin (1.0%), and acrylate-based compounds (1.0% each for polyacrylate and poly(octadecyl acrylate)) may reflect contributions from industrial coatings, paints, and maritime activities (Gaylarde et al., 2021). Although fragments and films represented a minority of the total anthropogenic particles (approximately 6% of all items), their absolute concentrations are far from negligible.

In summary, the heterogeneity observed among the three cores likely reflects the combined effects of dynamic sea-ice processes, such as advection, brine convection, atmospheric deposition, and local mixing. The presence of a clear vertical pattern in one of the three cores analyzed contrasts with most previous studies, which generally reported no significant stratification in MP or MF distribution (Peeken et al., 2018; Geilfus et al., 2019; Kanhai et al., 2020; Kelly et al., 2020; Kim et al., 2021; Ohno et al., 2024).

In our case, we hypothesize that the stratification observed in core T15-K4, with peak particle concentrations in the middle layers, may result from specific physical mechanisms during ice growth and evolution. During initial ice formation, particles suspended in the water column can be incorporated into the ice matrix and subsequently redistributed by brine drainage and convection as the ice thickens and ages (Chubarenko et al., 2022). The middle-layer enrichment could therefore results from a combination of processes, including: (a) preferential retention of particles within zones of reduced permeability and

redistribution associated with brine channel dynamics, such as in the case of the well described granular-to-columnar ice transition zone, where changes in pore structure may limit further vertical migration (Galley et al., 2015); (b) accumulation from below during periods of rapid ice growth at the ice-water interface, followed by partial upward displacement via brine channel convection (Khatmullina and Chubarenko, 2021); or (c) post-depositional redistribution during transient warming events, which can enhance brine channel connectivity and mobilize smaller particles (Bocherikova et al., 2026). In contrast, the absence of clear stratification in cores T13-K1 and T15-K2 may indicate more efficient vertical mixing within the ice, possibly related to higher initial ice permeability, different ice crystal structure, or localized differences in under-ice hydrodynamics and particle supply. Noteworthy, the bottom-layer enrichment observed aligns with incorporation from underlying seawater during ice growth, while surface inputs from atmospheric deposition appeared minimal, as suggested by the lack of statistically significant enrichment in the uppermost layers.

4.4. Methodological considerations on the identification of cellulosic fibers

A critical analytical challenge in FTIR-based identification is the distinction between natural celluloses (e.g., cotton) and man-made semi-synthetic cellulosic fibers (e.g., rayon/viscose) (Cai et al., 2019). As showed in the recent literature, their spectra often exhibit overlapping absorption bands, making straightforward classification difficult. Loof et al. (2016) clearly demonstrated this issue, showing that signals from chemical treatments partially overlap with the characteristic C—O, C—C, and C—H stretching vibrations of cellulose. To address this, Cai et al. (2019) proposed a practical solution by identifying a specific spectral marker: the band at approximately 1105 cm^{-1}, assigned to the C—O antisymmetric in-plane stretching. This band was found to be consistently present in natural celluloses even after aggressive treatments, while it was absent in semi-synthetic fibers such as rayon. However, the reliable application of this marker requires a careful, peak-by-peak inspection of each spectrum, which can be time-consuming and could bring errors when analyzing large datasets. Moreover, in highly weathered environmental samples, the 1105 cm^{-1} band may become less defined or shifted, further complicating the classification (Cai et al., 2019). For these reasons, and to avoid potential misclassifications, we adopted a conservative but robust approach that is widely adopted in the literature (e.g. in Peeken et al., 2018; Cai et al., 2019; Suaria et al., 2020; Athey and Erdle, 2022) and it consists in grouping all cellulosic fibers (both natural and semi-synthetic) into a single unified category ("cellulose/rayon"). This methodological choice implies that our reported abundances for the "cellulose/rayon" category represent the sum of both fractions (Fig. 5), and should be compared with caution against studies that attempt a more detailed (but potentially less certain) separation.

5. Conclusions

New insights into the presence and composition of microplastics (MPs) and microfibers (MFs) in first-year sea ice from Amur Bay, Sea of Japan were provided. The independently analyzed ice cores revealed a clear predominance of MFs, particularly those of cellulosic origin. The vertical distribution of MPs and MFs varied among cores, reflecting the heterogeneous and dynamic nature of sea-ice formation and brine channel connectivity, with occasional evidence of stratification. Overall, the collected results clearly highlight the need to include non-synthetic fibers in the monitoring of marine anthropogenic pollution, as growing evidence indicates that these materials can also exert biological and chemical impacts on marine organisms and ecosystems. At the same time, the consistent detection of MPs, although less abundant than non-synthetic MFs, demonstrates that coastal first-year sea ice can act as a significant temporary sink for different types of microparticles. Future research should aim to elucidate the fate of MFs during ice melt and to assess the potential adverse implications for polar and subpolar marine ecosystems.

CRediT authorship contribution statement

Davide Riseri: Writing – original draft, Formal analysis. **Irina Chubarenko:** Writing – original draft, Supervision, Methodology, Funding acquisition. **Alexander Lazaryuk:** Writing – original draft, Methodology, Investigation, Formal analysis. **Marina Lasagni:** Software, Funding acquisition. **Elena Collina:** Resources, Funding acquisition. **Francesco Saliu:** Writing – original draft, Supervision, Conceptualization.

Declaration of competing interest

The authors declare that they have no known competing financial interests or personal relationships that could have appeared to influence the work reported in this paper.

Acknowledgements

We dedicate this work to our friend, colleague, and coauthor, Irina Chubarenko, whose wisdom and leadership guided us along the way. Beyond her invaluable scientific guidance, she illuminated our lives with her passion for science, her deep love for nature, and her contagious warmth and enthusiasm.

Appendix A. Supplementary data

Supplementary data to this article can be found online at https://doi.org/10.1016/j.marpolbul.2026.119590.

Data availability

Data will be made available on request.

References

Aoki, K., Furue, R., 2021. A model for the size distribution of marine microplastics: a statistical mechanics approach. PLoS One 16 (11), e0259781. https://doi.org/10.1371/journal.pone.0259781.

Athey, S.N., Erdle, L.M., 2022. Are we underestimating anthropogenic microfiber pollution? A critical review of occurrence, methods, and reporting. Environ. Toxicol. Chem. 41, 822–837. https://doi.org/10.1002/etc.5173.

Athey, S.N., Carney Almroth, B., Granek, E.F., Hurst, P., Tissot, A.G., Weis, J.S., 2022. Unraveling physical and chemical effects of textile microfibers. Water 14 (23), 3797. https://doi.org/10.3390/w14233797.

Baitimirova, M., Katkevics, J., Baumane, L., Bakis, E., Viksna, A., 2013. Characterization of functional groups of airborne particulate matter. IOP Conf. Ser. Mater. Sci. Eng. 49, 012025. https://doi.org/10.1088/1757-899X/49/1/012025.

Bocherikova, I., Gorbachev, A., Chubarenko, I., 2026. Vertical re-distribution of microplastics particles in sea ice due to cooling/warming cycles: a laboratory experiment. Mar. Pollut. Bull. 224, 119136. https://doi.org/10.1016/j.marpolbul.2025.119136.

Browne, M.A., Dissanayake, A., Galloway, T.S., Lowe, D.M., Thompson, R.C., 2008. Ingested microscopic plastic translocates to the circulatory system of the mussel, Mytilus edulis (L). Environ. Sci. Technol. 42 (13), 5026–5031. https://doi.org/10.1021/es800249a.

Browne, M.A., Crump, P., Nivens, S.J., Terten, E., Tonkín, A., Galloway, T., Thompson, R., 2011. Accumulation of microplastic on shorelines worldwide: sources and sinks. Environ. Sci. Technol. 45, 9175–9179. https://doi.org/10.1021/es201811s.

Cai, H., Du, F., Li, L., Li, B., Li, J., Shi, H., 2019. A practical approach based on FT-IR spectroscopy for identification of semi-synthetic and natural celluloses in microplastic investigation. Sci. Total Environ. 669, 692–701. https://doi.org/10.1016/j.scitotenv.2019.03.124.

Callaghan, P.T., Eccles, C.D., 1996. NMR studies on antarctic sea ice. Bull. Magn. Reson. 18 (1–2), 62–64.

Chubarenko, I., 2022. Physical processes behind interactions of microplastic particles with natural ice. Environ. Sci. Commun. 4, 012001. https://doi.org/10.1088/2515-7620/ac49a8.

Chubarenko, I., Lazaryuk, A., Orlova, T., Lobchuk, O., Raguso, C., Zyubin, A., Lasagni, M., Saliu, F., 2022. Microplastics in the first-year sea ice of the Novik Bay,

Sea of Japan. Mar. Pollut. Bull. 185, 114236. https://doi.org/10.1016/j.marpolbul.2022.114236.
Chubarenko, I., Bocherikova, I., Esiukova, E., Isachenko, I., Kupriyanova, A., Lobchuk, O., Fetisov, S., 2023. Microplastics in sea ice: a fingerprint of bubble flotation. Sci. Total Environ. 891, 164611. https://doi.org/10.1016/j.scitotenv.2023.164611.
Cole, M., Lindeque, P., Fileman, E., Halsband, C., Goodhead, R., Moger, J., Galloway, T., 2013. Microplastic ingestion by zooplankton. Environ. Sci. Technol. 47, 6646–6655. https://doi.org/10.1021/es400663f.
Comnea-Stancu, I.R., Wieland, K., Ramer, G., Schwaighofer, A., Lendl, B., 2017. On the identification of rayon/viscose as a major fraction of microplastics in the marine environment: discrimination between natural and manmade cellulosic fibers using Fourier transform infrared spectroscopy. Appl. Spectrosc. 71, 939–950. https://doi.org/10.1177/0003702816660725.
Courtene-Jones, W., De Falco, F., Burgevin, F., Handy, R.D., Thompson, R.C., 2024. Are biobased microfibers less harmful than conventional plastic microfibers: evidence from earthworms. Environ. Sci. Technol. 58 (46), 20366–20377. https://doi.org/10.1021/acs.est.4c05856.
Cózar, A., Echevarría, F., González-Gordillo, J.I., Irigoien, X., Úbeda, B., Hernández-León, S., Palma, Á.T., Navarro, S., García-de-Lomas, J., Ruiz, A., Fernández-de-Puelles, M.L., Duarte, C.M., 2014. Plastic debris in the open ocean. Proc. Natl. Acad. Sci. USA 111 (28), 10239–10244. https://doi.org/10.1073/pnas.1314705111.
De Falco, F., Di Pace, E., Cocca, M., Avella, M., 2018. Evaluation of microplastic release caused by textile washing processes of synthetic fabrics. Environ. Pollut. 236, 916–925. https://doi.org/10.1016/j.envpol.2017.10.057.
Dethleff, D., Kempema, E.W., Koch, R., Chubarenko, I., 2009. On the helical flow of langmuir circulation – approaching the process of suspension freezing. Cold Reg. Sci. Technol. 56 (1), 50–57. https://doi.org/10.1016/j.coldregions.2008.10.002.
Détrée, C., Labbé, C., Paul-Pont, I., Prado, E., El Rakwe, M., Thomas, L., Delorme, N., Le Goïc, N., Huvet, A., 2023. On the horns of a dilemma: evaluation of synthetic and natural textile microfibre effects on the physiology of the Pacific oyster Crassostrea gigas. Environ. Pollut. 331, 121861. https://doi.org/10.1016/j.envpol.2023.121861.
dos Santos, J.B., Choueri, R.B., dos Santos, F.E.M., Santos, L.A.d.O., da Silva, L.F., Nobre, C.R., Cardoso, M.A., de Britto Mari, R., Simões, F.R., Delvalls, T.A., Gusso-Choueri, P.K., 2024. Are microfibers a threat to marine invertebrates? A sea urchin toxicity assessment. Toxics 12 (10), 753. https://doi.org/10.3390/toxics12100753.
Dris, R., Gasperi, J., Saad, M., Mirande, C., Tassin, B., 2016. Synthetic fibers in atmospheric fallout: a source of microplastics in the environment? Mar. Pollut. Bull. 104 (1–2), 290–293. https://doi.org/10.1016/j.marpolbul.2016.01.006.
Dris, R., Gasperi, J., Rocher, V., Tassin, B., 2018. Synthetic and non-synthetic anthropogenic fibers in a river under the impact of Paris Megacity: sampling methodological aspects and flux estimations. Sci. Total Environ. 618, 157–164. https://doi.org/10.1016/j.scitotenv.2017.11.009.
Eriksen, M., Lebreton, L.C.M., Carson, H.S., Thiel, M., Moore, C.J., Borerro, J.C., Galgani, F., Ryan, P.G., Reisser, J., 2014. Plastic pollution in the world's oceans: more than 5 trillion plastic pieces weighing over 250,000 tons afloat at sea. PLoS One 9 (12), e111913. https://doi.org/10.1371/journal.pone.0111913.
Friesen, L.W., Granberg, M.E., Pavlova, O., Magnusson, K., Hasselløv, M., Gabrielsen, G. W., 2020. Summer sea ice melt and wastewater are important local sources of microlitter to svalbard waters. Environ. Int. 139. https://doi.org/10.1016/j.envint.2020.105511.
Gago, J., Carretero, O., Filgueiras, A.V., Viñas, L., 2018. Synthetic microfibers in the marine environment: a review on their occurrence in seawater and sediments. Mar. Pollut. Bull. 127, 365–376. https://doi.org/10.1016/j.marpolbul.2017.11.070.
Galley, R.J., Else, B., Geilfus, N., Hare, A., Isleifson, D., Barber, D.G., Rysgaard, S., 2015. Imaged brine inclusions in young sea ice—shape, distribution and formation timing. Cold Reg. Sci. Technol. 111, 39–48. https://doi.org/10.1016/j.coldregions.2014.12.011.
Gaylarde, C.C., Neto, J.A.B., da Fonseca, E.M., 2021. Paint fragments as polluting microplastics: a brief review. Mar. Pollut. Bull. 162, 111847. https://doi.org/10.1016/j.marpolbul.2020.111847.
Geilfus, N., Munson, K.M., Sousa, J., Germanov, Y., Bhugaloo, S., Babb, D., Wang, F., 2019. Distribution and impacts of microplastic incorporation within sea ice. Mar. Pollut. Bull. 145, 463–473. https://doi.org/10.1016/j.marpolbul.2019.06.029.
Geminiani, L., Campione, F., Corti, C., Luraschi, M., Motella, S., Recchia, S., Rampazzi, L., 2022. Differentiating between natural and modified cellulosic fibres using ATR-FTIR spectroscopy. Heritage 5, 4114–4139. https://doi.org/10.3390/heritage5040213.
Golden, K.M., Eicken, H., Heaton, A.L., Miner, J., Pringle, D.J., Zhu, J., 2007. Thermal evolution of permeability and microstructure in sea ice. Geophys. Res. Lett. 34, L6501. https://doi.org/10.1029/2007GL030447.
Gomoyunov, K.A., 1927. Hydrological description of Amur Bay and the Suifuna River. In: Proizvoditel'nye sily Dal'nego Vostoka. Tr. 1-i konf., Vladivostok (Productive Forcexs of Far East. Proc. 1st Conf., Vladivostok), pp. 73–91.
Ikenoue, T., Yamada, M., Ishii, N., Kudo, N., Shirotani, Y., Ishida, Y., Kusakabe, M., 2022. Cesium-137 and $^{137}Cs/^{133}Cs$ atom ratios in marine zooplankton off the east coast of Japan during 2012–2020 following the Fukushima Dai-ichi nuclear power plant accident. Environ. Pollut. 311, 119962. https://doi.org/10.1016/j.envpol.2022.119962.
Ikenoue, T., Nakajima, R., Osafune, S., Siswanto, E., Honda, M.C., 2024. Vertical flux of microplastics in the deep subtropical Pacific Ocean: moored sediment-trap observations within the Kuroshio Extension recirculation gyre. Environ. Sci. Technol. 58, 16121–16130. https://doi.org/10.1021/acs.est.4c02212.
Isa, V., Saliu, F., Becchi, A., Spadaccino, G., Quinto, M., Veronelli, M., Lasagni, M., Galli, P., Lavorano, S., 2025. Impacts of microplastics on reef-building corals: disentangling the contribution of the chain scission products released by weathering. Sci. Total Environ. 975, 179239. https://doi.org/10.1016/j.scitotenv.2025.179239.
Ivleva, N.P., 2021. Chemical analysis of microplastics and nanoplastics: challenges, advanced methods, and perspectives. Chem. Rev. 121, 11886–11936. https://doi.org/10.1021/acs.chemrev.1c00178.
Jambeck, J.R., et al., 2015. Plastic waste inputs from land into the ocean. Science 347, 768–771. https://doi.org/10.1126/science.1260352.
Ji, X., Liu, J., Shen, J., Su, P., Liang, J., Feng, X., Liu, X., Liu, R., 2024. Characterization of chemical additives in daily clothing regarding human exposure and environmental emissions. Environ. Sci. Technol. Lett. 11 (6), 619–625. https://doi.org/10.1021/acs.estlett.4c00297.
Jiang, N., Chang, X., Huang, W., Khan, F.U., Fang, J.K.-H., Hu, M., Xu, E.G., Wang, Y., 2024. Physiological response of mussel to rayon microfibers and PCB's exposure: overlooked semi-synthetic micropollutant? J. Hazard. Mater. 470, 134107. https://doi.org/10.1016/j.jhazmat.2024.134107.
Jolly, D.J., Allen, E., Olah-Kovacs, B., McIlwraith, H., Warren, R.J., Woodhouse, C., Staines, M., Wright, A.C.M., Boots, B., Tolhurst, T.J., Green, D.S., 2025. Eco-friendly or eco-threat? The environmental risks of natural and semi-synthetic fibers. Environ. Res. Commun. 7 (5), 052502. https://doi.org/10.1088/2515-7620/add860.
Kanhai, L.D.K., Gardfeldt, K., Krumpen, T., Thompson, R.C., O'Connor, I., 2020. Microplastics in sea ice and seawater beneath ice floes from the arctic ocean. Sci. Rep. 10, 5004. https://doi.org/10.1038/s41598-020-61948-6.
Kansiz, M., Prater, C., Dillon, E.P., Lo, M., Anderson, J., Marcott, C., Kunkel, G., 2020. Optical photothermal infrared microspectroscopy with simultaneous Raman – a new non-contact failure analysis technique for identification of <10 μm organic contamination. Microsc. Today 28 (3), 26–35. https://doi.org/10.1017/S1551929520000917.
Kelly, A., Lannuzel, D., Rodemann, T., Meiners, K.M., Auman, H.J., 2020. Microplastic contamination in east antarctic sea ice. Mar. Pollut. Bull. 154, 111130. https://doi.org/10.1016/j.marpolbul.2020.111130.
Khatmullina, L., Chubarenko, I., 2021. Thin synthetic fibers sinking in still and convectively mixing water: laboratory experiments and projection to oceanic environment. Mar. Pollut. Bull. 288, 117714. https://doi.org/10.1016/j.envpol.2021.117714.
Kim, S.-K., Lee, H.-J., Kim, J.-S., Kang, S.-H., Yang, E.-J., Cho, K.-H., Tian, Z., Andrady, A., 2021. Importance of seasonal sea ice in the western arctic ocean to the arctic and global microplastic budgets. J. Hazard. Mater. 418, 125971. https://doi.org/10.1016/j.jhazmat.2021.125971.
Krembs, C., Gradinger, R., Spindler, M., 2000. Implications of brine channel geometry and surface area for the interaction of sympagic organisms in arctic sea ice. J. Exp. Mar. Biol. Ecol. 243, 55–80.
Lebedev, A.A., Tikhonova, O.A., Chaika, V.V., Kirianov, A.V., Khristophorova, N.K., Pikula, K.S., Shevchenko, V.P., Golokhvast, K.S., 2017. Coal terminal impact on marine suspension composition: Naknodka gulf (Sea of Japan). Proc. Russ. State Hydrometeorol. Univ. 48, 195–201 (in Russian).
Liu, J., Yang, Y., Ding, J., Zhu, B., Gao, W., 2019. Microfibers: a preliminary discussion on their definition and sources. Environ. Sci. Pollut. Res. 26 (29), 29497–29501. https://doi.org/10.1007/s11356-019-06265-w.
Loof, D., Hiller, M., Oschkinat, H., Koschek, K., 2016. Quantitative and qualitative analysis of surface modified cellulose utilizing TGA-MS. Materials 9 (6), 415. https://doi.org/10.3390/ma9060415.
Lotsiya, 1996. Lotsiya severo-zapadnogo berega Yaponskogo morya (Sailing Directions for the Northwestern Coast of the Sea of Japan). Gl. Upr. Navig. Okeanogr. Minist. Oborony, St. Petersburg.
Lusher, A.L., Burke, A., O'Connor, I., Officer, R., 2014. Microplastic pollution in the Northeast Atlantic Ocean: validated and opportunistic sampling. Mar. Pollut. Bull. 88, 325–333. https://doi.org/10.1016/j.marpolbul.2014.08.023.
Lyulin, S.V., Gurtovenko, A.A., Saliu, F., Galli, P., Surroop, D., Yaroslavov, A.A., Radionova, S.G., Kuznetsova, T.A., Kenny, J.M., 2025. Microplastics in the environment: the role of polymer science. Sci. Total Environ. 998, 180267. https://doi.org/10.1016/j.scitotenv.2025.180267.
Mel'nichenko, N.A., Tyveev, A.V., Savchenko, V.E., Kustova, E.V., 2019. Vertical distribution of brine and volume structure of thin annual ice in Amursky Bay based on the methods of nuclear magnetic resonance and magnetic resonance imaging. Oceanology 59 (5), 777–786. https://doi.org/10.1134/S0001437019050126.
Napper, I.E., Thompson, R.C., 2016. Release of synthetic microplastic plastic fibres from domestic washing machines: effects of fabric type and washing conditions. Mar. Pollut. Bull. 112 (1–2), 39–45. https://doi.org/10.1016/j.marpolbul.2016.09.025.
Obbard, R.W., Sadri, S., Wong, Y.Q., Khitun, A.A., Baker, I., Thompson, R.C., 2014. Global warming releases microplastic legacy frozen in Arctic Sea ice. Earth's Future 2 (6), 315–320. https://doi.org/10.1002/2014EF000240.
Ohno, H., Iizuka, Y., Fujii, Y., 2024. Microplastics in sea ice drifted to the Shiretoko Peninsula, the southern end of the Sea of Okhotsk. Sci. Rep. 14, 6304. https://doi.org/10.1038/s41598-024-78108-9.
Peeken, I., Primpke, S., Beyer, B., Gütermann, J., Katlein, C., Krumpen, T., Bergmann, M., Hehemann, L., Gerdts, G., 2018. Arctic sea ice is an important temporal sink and means of transport for microplastic. Nat. Commun. 9, 1505. https://doi.org/10.1038/s41467-018-03825-5.
Periyasamy, A.P., Tehrani-Bagha, A., 2022. A review on microplastic emission from textile materials and its reduction techniques. Polym. Degrad. Stab. 199, 109901. https://doi.org/10.1016/j.polymdegradstab. 2022.109901.
Petrenko, V.S., Manuilov, V.A., 1988. Fizicheskaya geografiya zaliva Petra Velikogo (Physical Geography of Peter the Great Bay). Dal'nevost. Gos. Univ., Vladivostok.
PlasticsEurope, 2024. PlasticsEurope Market Research Group (PEMRG) and Conversio Market & Strategy GmbH.

Podorvanova, N.F., Ivashinnikova, T.S., Petrenko, V.S., et al., 1989. Osnovnye cherty gidrokhimii zaliva Petra Velikogo (Yaponskoye more) (Main Features of Hydrochemistry of Peter the Great Bay, Sea of Japan). Dal'nevost. Otd. Akad. Nauk SSSR, Vladivostok.

Primpke, S., Dias, P.A., Gerdts, G., 2019. Automated identification and quantification of microfibres and microplastics. Anal. Methods 11 (16), 2138–2147. https://doi.org/10.1039/C9AY00126C.

Provencher, J.F., Ammendolia, J., Rochman, C.M., Mallory, M.L., 2019. Assessing plastic debris in aquatic food webs: what we know and don't know about uptake and trophic transfer. Environ. Rev. 27 (3), 304–317. https://doi.org/10.1139/er-2018-0079.

Remy, F., Collard, F., Gilbert, B., Compère, P., Eppe, G., Lepoint, G., 2015. When microplastic is not plastic: the ingestion of artificial cellulose fibers by macrofauna living in seagrass macrophytodetritus. Environ. Sci. Technol. 49 (18), 11158–11166. https://doi.org/10.1021/acs.est.5b02005.

Saliu, F., Montano, S., Lasagni, M., Galli, P., 2020. Biocompatible solid-phase microextraction coupled to liquid chromatography triple quadrupole mass spectrometry analysis for the determination of phthalates in marine invertebrate. J. Chromatogr. A 1618, 460852. https://doi.org/10.1016/j.chroma.2020.460852.

Saliu, F., Lasagni, M., Andò, S., et al., 2023. A baseline assessment of the relationship between microplastics and plasticizers in sediment samples collected from the Barcelona continental shelf. Environ. Sci. Pollut. Res. 30, 36311–36324. https://doi.org/10.1007/s11356-022-24772-1.

Sanchez-Vidal, A., Thompson, R.C., Canals, M., de Haan, W.P., 2018. The imprint of microfibres in southern European deep seas. PLoS One 13 (11), e0207033. https://doi.org/10.1371/journal.pone.0207033.

Siddiqui, S., Hutton, S.J., Dickens, J.M., Pedersen, E.I., Harper, S.L., Brander, S.M., 2023. Natural and synthetic microfibers alter growth and behavior in early life stages of estuarine organisms. Front. Mar. Sci. 9, 991650. https://doi.org/10.3389/fmars.2022.991650.

Sillanpää, M., Sainio, P., 2017. Release of polyester and cotton fibers from textiles in machine washings. Environ. Sci. Pollut. Res. 24 (23), 19313–19321. https://doi.org/10.1007/s11356-017-9621-1.

Silva, L.I., Ronda, A.C., Sosa Morales, M.C., Tomba, J.P., 2024. Practical guidelines and challenges in the isolation and characterization of microplastics/microfibers by Raman microscopy. Mar. Pollut. Bull. 209, 117133. https://doi.org/10.1016/j.marpolbul.2024.117133.

Song, Y.K., Hong, S.H., Jang, M., Han, G.M., Jung, S.W., Shim, W.J., 2017. Combined effects of UV exposure duration and mechanical abrasion on microplastic fragmentation by polymer type. Environ. Sci. Technol. 51 (8), 4368–4376. https://doi.org/10.1021/acs.est.6b06155.

Stanton, T., Johnson, M., Nathanail, P., MacNaughtan, W., Gomes, R.L., 2019. Freshwater and airborne textile fibre populations are dominated by 'natural', not microplastic, fibres. Sci. Total Environ. 666, 377–389. https://doi.org/10.1016/j.scitotenv.2019.02.278.

Stanton, T., James, A., Prendergast-Miller, M.T., Peirson-Smith, A., KeChi-Okafor, C., Gallidabino, M.D., Namdeo, A., Sheridan, K.J., 2024. Natural fibers: why are they still the missing thread in the textile fiber pollution story? Environ. Sci. Technol. 58 (29), 12763–12766. https://doi.org/10.1021/acs.est.4c05126.

Suaria, G., Avio, C., Mineo, A., et al., 2016. The Mediterranean Plastic Soup: synthetic polymers in Mediterranean surface waters. Sci. Rep. 6, 37551. https://doi.org/10.1038/srep37551.

Suaria, G., Achtypi, A., Perold, V., Lee, J.R., Pierucci, A., Bornman, T.G., Aliani, S., Ryan, P.G., 2020. Microfibers in oceanic surface waters: a global characterization. Sci. Adv. 6 (23), eaay8493. https://doi.org/10.1126/sciadv.aay8493.

Talley, L.D., Lobanov, V., Ponomarev, V., Salyuk, A., Tishchenko, P., Zhabin, I., Riser, S., 2003. Deep convection and brine rejection in the Japan Sea. Geophys. Res. Lett. 30, 1159. https://doi.org/10.1029/2002GL016451.

Taylor, M.L., Gwinnett, C., Robinson, L.F., Woodall, L.C., 2016. Plastic microfibre ingestion by deep-sea organisms. Sci. Rep. 6, 33997. https://doi.org/10.1038/srep33997.

Thompson, R.C., Olsen, Y., Mitchell, R.P., Davis, A., Rowland, S.J., John, A.W., McGonigle, D., Russell, A.E., 2004. Lost at sea: where is all the plastic? Science 304 (5672), 838. https://doi.org/10.1126/science.1094559.

Treilles, R., Cayla, A., Gaspéri, J., Strich, B., Ausset, P., Tassin, B., 2020. Impacts of organic matter digestion protocols on synthetic, artificial and natural raw fibers. Sci. Total Environ. 748, 141230. https://doi.org/10.1016/j.scitotenv.2020.141230.

Wayman, C., Niemann, H., 2021. The fate of plastic in the ocean environment – a minireview. Environ. Sci. Process Impacts 23 (2), 198–212. https://doi.org/10.1039/d0em00446d.

Weinstein, J.E., Crocker, B.K., Gray, A.D., 2016. From macroplastic to microplastic: degradation of high-density polyethylene, polypropylene, and polystyrene in a salt marsh habitat. Environ. Toxicol. Chem. 35 (7), 1632–1640. https://doi.org/10.1002/etc.3432.

Woodall, L.C., Sanchez-Vidal, A., Canals, M., Paterson, G.L.J., Coppock, R., Sleight, V., Calafat, A., Rogers, A.D., Narayanaswamy, B.E., Thompson, R.C., 2014. The deep sea is a major sink for microplastic debris. R. Soc. Open Sci. 1, 140317. https://doi.org/10.1098/rsos.140317.

Woodall, L.C., Gwinnett, C., Packer, M., Thompson, R.C., Robinson, L.F., Paterson, G.L.J., 2015. Using a forensic science approach to minimize environmental contamination and to identify microfibres in marine sediments. Mar. Pollut. Bull. 95 (1), 40–46. https://doi.org/10.1016/j.marpolbul.2015.04.044.

Zhang, K., Hamidian, A.H., Tubić, A., Zhang, Y., Fang, J.K.H., Wu, C., Lam, P.K.S., 2021. Understanding plastic degradation and microplastic formation in the environment: a review. Environ. Pollut. 274, 116554. https://doi.org/10.1016/j.envpol.2021.116554.